Electrochemical Formation of Photoactive Organic Heterojunctions. Porphyrin-C_{60} Polymeric Photoelectrochemical Cells.

Claudia Solis , Javier E. Durantini , Lorena Macor , Daniel A. Heredia , Edwin J. Gonzalez Lopez , Edgardo N. Durantini , María I. Mangione , Jörg Rappich , Thomas Dittrich , Luis Otero , Miguel Gervaldo

PII: S0013-4686(20)31726-6
DOI: https://doi.org/10.1016/j.electacta.2020.137333
Reference: EA 137333

To appear in: *Electrochimica Acta*

Received date: 3 August 2020
Revised date: 25 September 2020
Accepted date: 19 October 2020

Please cite this article as: Claudia Solis , Javier E. Durantini , Lorena Macor , Daniel A. Heredia , Edwin J. Gonzalez Lopez , Edgardo N. Durantini , María I. Mangione , Jörg Rappich , Thomas Dittrich , Luis Otero , Miguel Gervaldo , Electrochemical Formation of Photoactive Organic Heterojunctions. Porphyrin-C_{60} Polymeric Photoelectrochemical Cells., *Electrochimica Acta* (2020), doi: https://doi.org/10.1016/j.electacta.2020.137333

Highlights

- Donor-acceptor heterojunctions were formed by electrochemical polymerization.
- Photoinduced charge separation was observed in electropolymerized heterojunctions.
- Photogenerated electrons travelled to the external C_{60} layer and holes to the inner layer.
- The heterojunctions were used as photoactive materials in photoelectrochemical cells.
- Photoelectrochemical cells were able to reduce electron acceptors under illumination.

Electrochemical Formation of Photoactive Organic Heterojunctions. Porphyrin-C_{60} Polymeric Photoelectrochemical Cells.

Claudia Solis[a], Javier E. Durantini[a], Lorena Macor[a], Daniel A. Heredia[b], Edwin J. Gonzalez Lopez[b], Edgardo N. Durantini[b], María I. Mangione[c], Jörg Rappich[d], Thomas Dittrich[d], Luis Otero[a,*], Miguel Gervaldo[a,*].

a IITEMA-CONICET, Departamento de Química, Universidad Nacional de Río Cuarto-CONICET Agencia Postal Nro. 3, X5804BYA Río Cuarto, Córdoba, Argentina.

b IDAS-CONICET, Departamento de Química, Universidad Nacional de Río Cuarto-CONICET Agencia Postal Nro. 3, X5804BYA Río Cuarto, Córdoba, Argentina.

c IQUIR-CONICET, Facultad de Ciencias Bioquímicas y Farmacéuticas, Universidad Nacional de Rosario, Suipacha 531, S2002LRK Rosario, Argentina.

d Helmholtz-Zentrum Berlin für Materialien und Energie GmbH, Institut für Silizium-Photovoltaik, Kekuléstr. 5, 12489 Berlin, Germany.

* Corresponding authors:

E-mail address: mgervaldo@exa.unrc.edu.ar,

E-mail address: lotero@exa.unrc.edu.ar,

Abstract:

Fully polymeric donor-acceptor organic-organic heterojunctions were successfully formed by successive electrochemical polymerization steps. C_{60} holding polymer acted as an electron acceptor layer when it was electrochemically deposited on the top of a porphyrin based conducting polymer with dendrimeric structure. Porphyrin fluorescence emission quenching and energy dependent surface photovoltage analysis demonstrated that the heterojunctions produced photoinduced charge separated states. Also, it was found that after irradiation of heterojunctions the photogenerated electrons traveled to the C_{60} external surface, while the holes moved to the inner hole transport layer. When the heterojunctions were used in photoelectrochemical cells, the generated light-induced charge separated states were able to electrochemically reduce electron acceptors in aqueous media.

Keywords:

Heterojunctions, Electropolymerization, Charge separated states, Photoelectrochemical cell.

1. Introduction

Solar energy conversion and storage using photoelectrochemical systems based on organic materials is one of the most attractive strategies in the development of versatile, efficient and cost-effective devices [1-3]. This is mainly due to the synthetic versatility of the organic compounds, and the consequent tunability of the electronic and optical properties of the new materials [4,5]. However, the development and application of organic materials in optoelectronic devices is often a challenging task, because they must form thin films with suitable solid properties, satisfactory stability, efficient light absorption, adequate hole/electron transport capability, appropriate work function, and must also be cost competitive with the established technology [1,6]. In this frame, organic based energy conversion devices are basically formed by heterogeneous junctions, where the excitons generated by light absorption produce separated electrical charges [7,8]. These boundaries can be distributed in a bulk heterojunction fashion or in the limits of two thin layers. In both cases, an electron donor and hole transport material (HTM) is in contact with an electron acceptor that also acts as electron-transport material (ETM). There are several examples of the application of polymeric organic materials as both, HTM and ETM, and as building blocks in the development of high efficient organic solar cells that convert solar radiation into electrical energy [9-13]. However, there are few examples related to the use of organic-based energy conversion devices in the direct generation of solar fuels [14], possibly due to the low stability of the organic materials when they are immersed in liquid solutions and exposed to illumination under applied potentials. These are conditions where the photodegradation produces gradual damages to the device. One strategy applied to overcome this problem in aqueous media for direct solar generation of hydrogen is covering the organic layers with an amorphous TiO_x film and a catalytic surface (Pt) [15-17]. The Poly(3-hexylthiophene)/[6,6]-phenyl-C_{61}-butyric acid methyl ester organic blend based photocathode showed to be able of producing stable solar hydrogen with a faradaic efficiency of 100 % [18]. Another possible approach to increase the organic material stability when it is

in contact with liquid media is the use of fully polymeric arrangements [19], which can be produced by electrochemical polymerization. For example, Nasybulin et al. reported the formation of heterojunction solar cells by electrochemical co-deposition of poly(thieno[3,2-b]thiophene) and fullerene [20]. In a similar way, we have described the formation of organic photoactive heterojunctions by successive electrochemical polymerization of electron donor and electron acceptor layers [21-23].

Recently we have reported the synthesis of a dendrimeric porphyrin where the central core is connected to eight carbazole (CBZ) peripheral groups [24]. The electrochemically induced coupling reaction of the CBZ groups generated a conducting π-conjugate polymeric material (Fig. 1a). In this article we investigated the electrochemical generation of organic photoactive heterojunctions by the coupling of this hyperbranched π-conjugate system to CBZ-modified C_{60} (Fig. 1b) as electron acceptor. Also, a CBZ monomer was used for the electrochemical formation of a hole transport layer (Fig. 1c). Two photoelectrode arrangements were prepared (Fig. 1d) over Indium Tin Oxide (ITO) bare contact. In both cases a HTM layer was deposited over the bare ITO (dicarbazole layer (DCBZ)). In the first arrangement, the electron donor (porphyrin polymer layer, Porp) and electron acceptor (C_{60} polymer layer) were sequentially deposited generating the trilayer DCBZ/Porp/C_{60}. In the second arrangement, a mixed layer (Mix) was electrochemically deposited from a solution containing both, porphyrin and C_{60} monomers. Finally, a C_{60} layer was deposited on top of the second layer generating DCBZ/Mix/C_{60} arrangement. As shown in this work, these photoelectrodes are efficient for the generation of photoinduced charge separated states and suitable for the photoelectrochemical reduction of electron acceptors in aqueous media.

2. Experimental section

Materials, instrumentation and methods.

All commercially available chemicals were received in analytic grade without further

purification unless otherwise specified. m-CBZ, m-Porp and m-C_{60} monomers were synthesized as previously described [24,25] Dichloromethane (DCM) was purified by distillation with CaH_2 (50 g L^{-1}) as water removal agent. The indium tin oxide (ITO) coated glass substrates (Delta Technologies, nominal resistance 8−12 Ω/ square) were cleaned in an ultrasonic bath with acetone-isopropanol (50 vol.%), ethanol and deionized water, respectively, and then dried with nitrogen. UV-Vis absorption and fluorescence spectra were recorded on a UV-Visible Hewlett Packard -Diode Array 8453 spectrometer and on a FluoroMax-4, Horiba fluorometer, respectively. The electrochemical and spectroelectrochemical measurements were carried out with an Autolab potentiostat/galvanostat (Electrochemical Instruments) utilizing a three-electrode cell configuration at room temperature. The characterization of the redox processes and the electrochemical polymerization of the individual monomers have been previously reported [24,25]. In this work the multilayer photoelectrodes with different configuration were formed by successive electropolymerization processes on ITO electrodes. The multi-step electrochemical polymerization protocol involves the use of cyclic voltammetry (CV) technique, where the ITO based photoelectrodes act as working electrodes, a Pt wire as counter electrode, and Ag wire as quasi-reference electrode. The solutions used for the electrodeposition were prepared from either 0.5 mM m-CBZ or 0.5 mM m C_{60} or 0.05 mM m-Porp or a mixture of 0.05 mM m-Porp and 0.5 mM m-C_{60} together with 0.1 M tetrabutylammonium hexa-fluorophosphate ($TBAPF_6$) as supporting electrolyte dissolved in dichloromethane (DCM). All electrochemical polymerizations for the generation of the different layers were carried out applying ten CV cycles at 0.1 V s^{-1} in the potential range exhibited in the corresponding figure. After each electro-deposition of a layer, the electrodes were removed from the electrolytic cell and washed with solvent to remove remaining monomer, electrolyte and low-weight molecular species. UV-visible spectra were taken to the electrodes in order to assess the growing process of the different successive layers. The electrochemical responses of the polymeric multilayer films were carried out in all cases in monomer-free solvent

supporting electrolyte media. Ferrocene was used as an internal reference. All potentials are reported versus the potential for the saturated calomel electrode (SCE). High purity argon was used to remove dissolved oxygen for at least 15 min prior to each electrochemical processing.

Spectroelectrochemical experiments of the polymer-coated ITO electrodes were carried out in a cell built from a 10 mm commercial quartz UV-visible cuvette. The different ITO/Polymeric films were used as working electrodes, the Pt counter electrode was isolated from the solution by a glass frit, and an Ag wire as the quasi-reference electrode. The cell containing the DCM-$TBAPF_6$ solvent supporting electrolyte media was placed in the optical path of the sample light beam. The background correction was obtained by taking an UV–Vis spectrum of a blank cell (an electrochemical cell with an ITO working electrode without the polymeric film) with identical conditions and parameters. During the measurement, readings were taken as a function of time under kinetic control. Film thicknesses were estimated from the relation between film absorbance, film charge, and film thickness of the individual photoactive materials that form the heterojunction layers in DCBZ/Porp/C_{60} and DCBZ/Mix/C_{60} photoelectrodes (see SI for details). Scanning electron microscopy (SEM) images were performed with a field emission scanning electron microscope FE-SEM, Sigma Zeiss with an acceleration voltage of 5 kV.

The generation of photoinduced charge separated states in the different photoelectrodes configurations was studied by energy dependent modulated surface photovoltage (SPV) [26]. The SPV signals reflex the amount of generated charges by the incident light, and the distance between the centers of positive and negative charge distributions [22,23,27]. The SPV spectra were not normalized to the photon flux. Measurements were carried out in vacuum, in front illumination alignment. The fixed capacitor arrangement was used, with chopped monochromatic light (modulation frequency 6 Hz) obtained from a quartz prism monochromator (SPM2) and a 100 W halogen lamp. The measurements were carried out using the already described set-up [28].

Photoelectrochemical experiments were conducted in aqueous phosphate buffer (pH 7.5 or 4.5) solutions (0.1 M) with and without methyl viologen (MV^{+2} 0.05 M) depending on the experiment. These solutions were deoxygenated and the experiments were carried out under argon atmosphere. The photoelectrochemical measurements were performed under potentiostatic control (Palm Sens 4). Action spectra were obtained by illumination of the photoelectrodes with monochromatic light obtained from a 75 W high-pressure Xe lamp (Photon Technology Instrument, PTI) and a computer-controlled PTI high intensity grating monochromator (5 nm band width). The steady state photocurrents were obtained in front face configuration (illuminated area: 1 cm^2). The incident light intensities at different wavelengths were measured with a Coherent Laser-Mate Q radiometer.

3. Results and discussion

3.1. Electrochemical film formation and characterization

In order to produce the layers that form the different arrangements (DCBZ/Porp/C_{60} and DCBZ/Mix/C_{60}), (see Fig. 1d) cyclic voltammetry was used. In the construction of the photoelectrodes, each polymeric layer was grown using solutions of the desired monomer in solvent-support electrolyte media (see Fig. S2). Then, the films were washed and the electrochemical response of the electrogenerated films were obtained (in a solution containing only supporting electrolyte) and finally, their absorption spectra were measured. These procedures (electrochemical growing, electrochemical response, and absorption spectra recording) were repeated for each new posterior layer that was deposited.

Fig. 2 shows for the tri-layer (a, b, and c) and for the mixed layer structure (d, e, and f), the film growing cyclic voltammograms (a and d), the electrochemical responses measured in the solvent-electrolyte media (b and e), and the absorption spectra (c and f) registered after deposition of each of the three layers (depicted in Fig. 1d). The first cyclic voltammograms of m-CBZ in solution (Fig. 2a

and d, dotted black lines) are irreversible and present an oxidation peak at around 1.25 V, which can be assigned to the formation of the radical cation of CBZ and its coupling to form carbazole dimmers [29,30] (see Fig. S2 and Scheme I in Support Information, SI). After ten continuous cycles, the oxidation/reduction currents are increased, which indicates the formation and deposition of the DCBZ layers over the ITO electrodes (solid black lines). Their electrochemical responses in solvent-electrolyte media are characterized by two reversible redox peaks (Fig. 2b and e, black lines), and the absorption spectra of the DCBZ layers present a high absorption in the UV zone with a tail that extends to around 450 nm (Fig. 2c and f, black lines). All these results are consistent with the electrochemical formation of DCBZ conducting films (see Scheme I in SI) [29,30]. On the other hand, the red lines in Fig. 2a-f show the formation of the second polymeric layers (see Fig.1d), corresponding to the generation of porphyrin polymer (Fig. 2a-c) and Mix layers (m-Porp + m-C_{60}, Fig. 2d-f), over the corresponding DCBZ layer. After ten polymerization cycles (see Fig. S2) in m-Porp or m-Porp+m-C_{60} mixed solutions, the cyclic voltammograms present increases in the oxidation/reduction currents (Fig. 2a and d, red lines), and the electrochemical responses in monomer free solvent-electrolyte media are similar to the ones observed for DCBZ layers alone, but with higher oxidation/reduction peak currents (Fig. 2b and e, red lines), indicating that more electroactive material was deposited over the electrodes. The absorption spectra of the DCBZ/Porp and DCBZ/Mix layers, now present the Soret and Q bands at around 420 and 550 nm, typical of Zn porphyrins (Fig. 2c and f, red lines). There are also increases in the absorptions in the UV zone which are related to the absorption of carbazole dimmer units (generated during formation of the Porp and C_{60} layers), and also to the absorption of the C_{60} units [25]. Moreover, for DCBZ/Mix layer, the ratio between the absorption in the UV zone and the Soret band is higher compared to the same ratio in DCBZ/Porp, because of the contribution not only derivated from carbazole dimer units, but also from the C_{60} polymeric layer. Therefore, the occurrence of the Soret band confirms the deposition of Porp in both layers. The higher ratio between the absorptions in the

UV zone and the Porphyrin band observed for DCBZ/Mix related to DCBZ/Porp, proves the deposition of the Mix layer, over the DCBZ polymeric films. Finally, C_{60} polymeric films were electrochemically formed over DCBZ/Porp and DCBZ/Mix layers, respectively. After ten polymerization cycles in m-C_{60} solution (Fig. S2), the film growing cyclic voltammograms (Fig. 2a and d, blue lines) and their electrochemical responses (Fig. 2b and e, blue lines) present higher oxidation/reduction currents. Again, this behavior indicates the deposition of more electroactive material (C_{60} polymer) over the already formed bilayer structures. The absorption spectra of DCBZ/Porp/C_{60} and DCBZ/Mix/C_{60} layers (Fig. 2c and f, blue lines) still present the Soret and Q bands, these are now mounted over a tail that extends from the UV zone to around 600 nm, but the intensities of the Soret bands do not increase. This new tail that appears in the absorption spectra of DCBZ/Porp/C_{60} and DCBZ/Mix/C_{60} layers has been observed before and related to the absorption of the polymeric C_{60} layer deposited over bare ITO [25]. From the relation between film absorbance, film charge, and film thickness of the photoactive materials that form the heterojunction layers in DCBZ/Porp/C_{60} and DCBZ/Mix/C_{60} photoelectrodes, a thickness of around 250 nm can be estimated for both photoactive layers (see experimental section, SI, and Fig. S1). The top surface morphologies of DCBZ/Porp/C_{60} and DCBZ/Mix/C_{60} arrangements were investigated by SEM technique. It can be seen from the top view SEM images (Fig. S3) that the polymers completely cover the electrode surfaces, without pinholes and present a homogeneous surface formed by a random distribution of globular topographies. These characteristics are similar than those observed before when C_{60} was electrodeposited over bare ITO [25].

In order to gain more information about the deposition of the different layers, spectroelectrochemical studies were conducted [24,25]. For all configuration electrodes, absorption spectra at different applied potential values were obtained, then the absorption spectrum at 0.00 V was subtracted from each individual spectrum and plotted as ΔAbs. Fig. 3 exhibits the difference spectra obtained at the selected applied potentials corresponding to the first (Fig. 3a and c) and second (Fig. 3b

and d) oxidation peaks observed in the electrochemical responses of each polymeric layer (see the arrows in Fig. 2b and e). It can be seen that at the applied potential corresponding to the first oxidation peaks all layers present the development of an absorption band at around 410 nm, and a second one that starts at about 650 nm and extends to the IR region. The intensities of these bands are increased after deposition of the second (red lines) and third (blue lines) layers in comparison to the first ones (black lines), formed by DCBZ units. Additionally, at the applied potential corresponding to the second oxidation peaks (Fig. 3b and d), in all cases the layers present a broad absorption band between 500 and 850 nm. Again, the intensities of these bands are bigger after deposition of each new layer (red and blue lines). Also, it must be noted that, after deposition of the Porp or Mix layers (Fig. 3, red lines), a small bleaching of the Soret band is observed at the applied potential corresponding to the first oxidation peak (Fig. 3a and c). A complete bleaching of the Soret band is observed when the second oxidation peak is reached (Fig. 3b and d, red lines). This indicates that the porphyrin macrocycle gets oxidized in the DCBZ/Porp and DCBZ/Mix bilayer electrodes (generating the corresponding porphyrin radical cation) [31-33]. Moreover, bleaching of the Soret band is also observed after deposition of the C_{60} layers (Fig. 3, blue lines), demonstrating that the Porp layers are still electroactive and that the porphyrin core can be oxidized even with the C_{60} layer on top. Fig. S4 shows the difference absorption spectra for the complete DCBZ/Porp/C_{60} and DCBZ/Mix/C_{60} trilayers at several applied potentials. At applied potentials between 0.3 and 1.1 V, new bands at around 410 nm and a second one that extends to the IR zone appear. At more positive applied potentials, the bleaching of the porphyrin Soret band and a new positive band at around 650 nm are observed. It must be remarked that the bands observed at the first oxidation potential for DCBZ, Porp, and Mix layers (Fig. 3a and c) as well as the ones developed at applied potentials between 0.3 and 1.1 V (Fig. S4) all of them appear at the same wavelength values, and correlate with the absorption spectra of carbazole dimer radical cation [24,29,30]. In the same way, the bands observed at the second oxidation peak (Fig. 3b and d) and the ones that appear at applied

potentials higher than 1.1 V (Fig. S4) are all similar and related to the absorption spectra of carbazole dimer dication. Additionally, oxidation of the porphyrin macrocycle is confirmed by the Soret band bleaching, and by the apparition of a small new peak at around 700 nm, that is mounted over the broad band originated in the carbazole dimer oxidized species (Fig 3b and c red lines), being this band at 700 nm associated to the formation of porphyrin radical cation [31-33]. Fig. 4a-b shows the absorption changes observed at selected wavelengths obtained during the spectroelectrochemical experiments. The traces where Porphyrin (Soret band 420 nm), carbazole dimer radical cation (980 nm), DCBZ dication and porphyrin radical cation (760 nm) present absorptions [24,29-31,33] recovered their initial values after a complete CV cycle. This fact confirms that the oxidation-reduction processes are fully reversible in both DCBZ/Mix/C_{60} and DCBZ/Porp/C_{60} trilayer stacks.

All the electrochemical and spectroelectrochemical results are in agreement with the presence of carbazole dimmer units in each individual polymeric layer, which were formed by coupling of CBZ radical cations generated during electrochemical cycling (see Scheme I in SI). It is also probable that during electrochemical cycling some free CBZ units present in the first deposited DCBZ layer react with free CBZ units in Porp, generating a carbazole dimmer in-between. A similar coupling could occur between the CBZ units bonded to the Porp and to the C_{60} units present in each respective layer (Scheme II in SI). Although porphyrin radical cations are formed when the porphyrin cores are oxidized, these radical cations are stable and therefore, direct reaction between C_{60} and porphyrin oxidized species does not take place. The electrochemical response for all layers showed two oxidation peaks (Fig. 2b and e), associated to the oxidations of carbazole dimmers, which generate the corresponding radical cations and dications [30], as it was already reported for structural related based polymers [29,34]. Also, the absorption bands observed at the first oxidation peak correlate with the absorption spectra of carbazole dimer radical cation and the ones observed at the second oxidation peak are related to carbazole dimer dication and porphyrin radical cation [29-31,34]. Additionally, the

difference absorption spectra observed in Fig S4 (corresponding to the complete arrangements), also showed absorption spectra related to the above mentioned species, confirming that all layers maintain their electrochemical activities. Moreover, the absorption spectra of the DCBZ/Porp/C_{60} and DCBZ/Mix/C_{60} arrangements showed bands related to DCBZ, Porphyrin and C_{60} individual polymeric layers, respectively. The absorption spectra of the arrangements seem to consist of a linear combination of each individual layers [24,25].

3.2. Generation of photoinduced charge separated states.

As it was expected, Porp film exhibited light emission after excitation at the Soret and Q bands. This is because of the electrogenerated polymer dendrimeric structure, which avoids self-quenching originated by π stacking between the tetrapyrrolic macrocycle [24,35]. Fig. 5 shows the fluorescence spectrum of Porp film, which presents bands at very similar wavelength values respect to the monomer in solution, although the film exhibits a 5 nm red shift [24]. Also, when a Porp film is electrodeposited over a DCBZ layer the resulting bilayer (DCBZ/Porp) still presents a fluorescence emission intensity similar to that observed for Porp film alone, indicating that DCBZ layer does not affect the emission properties of Porp film. On the contrary, when a layer of C_{60} is deposited over the Porp film (Porp/C_{60}), the emission is almost suppressed (Fig. 5 blue line). Moreover, when a Mix layer is electrochemically generated (from a solution containing both Porphyrin and C_{60} monomers), the resulting Mix layer presents a very low emission (Fig. 5 black line). Also, a very low emission is observed when Mix layer is electrogenerated over DCBZ layer (DCBZ/Mix). The low emission observed in Mix, Porp/C_{60} and Mix/C_{60} layers indicates that C_{60} film quenches Porp fluorescence, probably due to a charge transfer mechanism, generating a charged separate state. This quenching mechanism has been observed in Porphyrin-C_{60} dyads and polymers [36-38].

The capacity to produce charge separated states and the direction in which these charges diffuse

were studied by SPV spectroscopy. SPV spectroscopy is a powerful tool that allows the study of photoinduced charge transfer generation and diffusion in photoactive thin films [21,39,40]. In general, the sign of the in-phase light-modulated SPV signal denotes the direction in which the photogenerated electrons are preferentially separated. When the sign of the in-phase SPV signal is negative, the photogenerated electrons are preferentially separated towards the external surface, while if the sign is positive the electrons will preferentially travel to the internal surface [21,39]. DCBZ/Porp bilayer film presents a very low and noisy SPV signal (Fig. 6a, red lines), showing that there is no detectable generation of photoinduced charge separation centers [21,39], in agreement with the observation of fluorescence emission in this film. On the contrary, when the C_{60} layer is present in DCBZ/Porp/C_{60} arrangement, it shows a low negative in-phase SPV signal and a remarkable positive phase-shifted by 90° signal (blue lines in Fig. 6a), indicating that the photogenerated electrons are separated in the direction of the external surface (C_{60} layer). In a similar way, in DCBZ/Mix bilayer arrangement, low SPV signals are observed, although in this case the signals are detectable (red lines in Fig. 6b). Thus, it is possible that the presence of both Porp (electron donor) and C_{60} (electron acceptor) in the Mix layer, generates photoinduced charge separated states. This result is in agreement with the fact that no emission fluorescence was observed in the DCBZ/Mix layer stack. Moreover, the SPV amplitude for the DCBZ/Mix/C_{60} layer stack (blue lines in Fig. 6b) is much higher compared to the amplitude values obtained for the DCBZ/Mix layer stack, and similar to that observed for DCBZ/Porp/C_{60} photoelectrodes (blue lines in Fig. 6a). Therefore, the presence of the C_{60} layers has a strong influence in the generation, diffusion and recombination of the photogenerated charge carriers.

All these results demonstrate that in both DCBZ/Mix/C_{60} and DCBZ/Porp/C_{60} trilayer photoelectrodes, charge separated states are generated after light absorption where positive charges (holes) are preferentially separated towards the internal layer, while the negative charges (electrons) move to the C_{60} external acceptor layer (see Fig. S5). Thus, it could be expected that in the presence of

an external sacrificial electron acceptor in solution, the electrochemical generated trilayer photoelectrodes were able to generate photoelectrochemical effects.

3.3. Photoelectrochemical properties

Photoelectrochemical cells in a three electrode configuration, formed by DCBZ/Porp/C_{60} and DCBZ/Mix/C_{60} photoelectrodes, were studied in aqueous phosphate buffer (pH 7.5) initially containing 0.05 M of methyl viologen cation (MV^{+2}) as sacrificial electron scavenger. Fig. 7a-c shows the incident-photon-to-photocurrent efficiency (IPCE% [41]) values obtained under constant applied potential (-0.20 V), when the photoelectrodes are irradiated with monochromatic light of different wavelengths. The bias potential was chosen at values where the stationary generated photocurrents reached a plateau in the photocurrent-applied potential curves (see Fig. S6). Photoelectrodes formed by only single layers of DCBZ, Porp, and C_{60} polymers were also studied in the same conditions for comparison. From Fig. 7a it is clearly observed that for DCBZ and C_{60} single polymeric layers the IPCE% values are very low and the layers present photoeffects only in the 300-450 nm range. On the contrary, in the case of the Porp-electropolymeric film, the action spectrum exhibits distinguishable photocurrent generation due to absorption at the porphyrin Soret and Q bands (420 and 550 nm). Additionally, a peak at 330 nm is observed, which is due to the electronic transition originated in the DCBZ moieties, showing their contribution to the photoelectrochemical effect. Furthermore, when a bilayer is formed (DCBZ/Porp photoelectrode), this material shows to be effective in the photocurrent generation, as it is expected due to the already described effect for the Porp film (see Fig. 7b and a). Also, in the bilayer DCBZ/Mix electrode, where the electron acceptor C_{60} is copolymerized with the porphyrin polymer (Fig. 7c), the IPCE% values are higher in comparison with the electrode only formed by the porphyrin electropolymer. However, when electropolymeric C_{60} acceptor layers are present in both DCBZ/Porp/C_{60} and DCBZ/Mix/C_{60} photoelectrodes, the IPCE%s reach values more

than three times higher than that obtained for the bilayer materials. Fig. 7b-c shows that both trilayer photoelectrodes are able to produce photoinduced charge separated states which, in contact with an electron acceptor in solution, generate stable photocurrents. This is in agreement with the effect observed by energy dependent surface photovoltage experiments, where the preferential accumulation of negative charge in the outer surface (C_{60}) and positive charge in the inner layers were demonstrated (see Fig. 6 and Fig. S5). Also, the well match between the absorption spectra of the films and the corresponding photocurrent action spectra indicates that the light absorption by the polymeric films is responsible for the observed photoeffects [41]. It must be noted that there is an extra band in the photocurrent action spectra in the 600-700 nm range that is not present in the absorption spectra of the heterojunctions. As it was mentioned above, under illumination charge separated states are generated forming porphyrin radical cations that present an absorption band in this region. Therefore, it is possible that these oxidized species can contribute to the observed IPCE. The above mentioned results demonstrate that in the trilayer photoelectrodes after light absorption, the electrons in the polymeric C_{60} outer layers are able to be transferred to an acceptor in aqueous solution. In the present conditions (phosphate buffer pH 7.5), the presence of a sacrificial electron scavenger is necessary to observe measurable photocurrents. The lack of MV^{+2} in the aqueous media drives to very low and transitory photoelectrical effects. On the contrary, when the aqueous electrolyte pH is adjusted at lower values (without MV^{+2}), the photocurrents generated by illumination of the trilayer photoelectrodes are increased respect to pH 7.5. Fig. 8a-b shows on-off illumination cycles under white light. The detected photocurrents are cathodic, indicating that the electrons are transferred from the electrodeposited layers to the aqueous solution. Fig. 9 shows the photocurrent action spectra for both DCBZ/Porp/C_{60} and DCBZ/Mix/C_{60} photoelectrodes obtained in aqueous NaH_2PO_4 (pH = 4.5). In both cases, the photocurrent action spectra match the absorption spectra of the films, confirming that the trilayer photoelectrodes are responsible for the observed photoeffect. It should be noted that the photocurrents

and the IPCE values for DCBZ/Porp/C_{60} are higher than those observed for DCBZ/Mix/C_{60}. After light absorption, charged separated states are generated and then they must separate and reach the corresponding interfaces. Another possibility is that these states recombine before they reach the interface with the electrolyte and therefore no photocurrent is produced. Therefore, the difference in the photocurrent and IPCE values could be due to a difference in the charge recombination rates of the different arrangements. Then, it is possible that the difference in photocurrent generation efficiency is originated in a higher recombination rate in DCBZ/Mix/C_{60} photoelectrode, which is probable due to the close contact between porphyrin electron donor and C_{60} electron acceptor in the Mix structure. For a better description of the observed photoeffects and the direction of the photocurrents, an energy diagram was constructed (Fig. 10) [18,21,41]. According to the observed results and taking into account the energetics of the trilayers and those related to MV^{+2} and H^{+} electron acceptors in aqueous solution, it is proposed that after light irradiation of the photoelectrodes, electrons from the Porp HOMO to the C_{60} LUMO and holes from the Porp to the DCBZ layer are transferred [36-38]. Then the holes move to the ITO base electrode and the electrons in the C_{60} LUMO are transferred to the MV^{+2} (pH=7.5) reducing the organic acceptor, or to the protons in the aqueous media (pH=4.5), allowing the photoelectrochemical generation of H_2.

4. Conclusions.

Multilayered donor-acceptor polymeric organic-organic heterojunctions were successfully formed by sequential electrochemical polymerization. The heterojunctions were formed by a DCBZ hole transport layer, donor porphyrin, and acceptor C_{60} polymeric layers respectively. The successive layers were electroactive and underwent reversible oxidation-reduction processes. Porphyrin donor polymer fluorescence emission was quenched by electron transfer to the C_{60} acceptor polymeric layer, generating charge separated states. SPV measurements demonstrated the formation of charge separated

states and also showed that the photogenerated electrons traveled to the C_{60} external polymeric layer while the holes moved to the DCBZ inner layer. The donor-acceptor heterojunctions were used in photoelectrochemical cells containing electron acceptors in aqueous media. Irradiation of the heterojunctions produced stable cathodic currents and photocurrent action spectra similar to the absorption spectra of the heterojunctions, showing that these were responsible of the observed photoeffects. These results demonstrate the potential application of the electrochemical generated donor-acceptor polymeric heterojunctions as building blocks for the development of solar energy devices.

Acknowledgements

Authors are grateful to Secretaría de Ciencia y Técnica, Universidad Nacional de Río Cuarto (Secyt-UNRC), Ministerio de Ciencia y Tecnología de la Provincia de Córdoba (MinCyT-Cba), Consejo Nacional de Investigaciones Científicas y Técnicas (CONICET) and Agencia Nacional de Promoción Científica y Tecnológica (ANPCYT) of Argentina for financial support.

Credit author statement.

Claudia Solis, Javier E. Durantini, Lorena Macor: Experimental work. Daniel A. Heredia, Edwin J. Gonzalez Lopez, Edgardo N. Durantini, María I. Mangione: Organic Synthesis. Jörg Rappich, Thomas Dittrich: SPV measurements. Luis Otero, and Miguel Gervaldo: Writing- Reviewing and Editing.

Declaration of interests

The authors declare that they have no known competing financial interests or personal relationships that could have appeared to influence the work reported in this paper.

REFERENCES

[1] H. Youn, H.J. Park, L.J. Guo, Organic photovoltaic cells: from performance improvement to manufacturing processes, Small, 11 (2015) 2228-2246.
[2] D. Di Carlo Rasi, R.A.J. Janssen, Advances in solution-processed multijunction organic solar cells, Adv. Mater., 31 (2019) 1806499.
[3] Y. Liu, Y. Chen, Integrated perovskite/bulk-heterojunction organic solar cells, Adv. Mater., 32 (2020) 1805843.
[4] S. Holliday, Y. Li, C.K. Luscombe, Recent advances in high performance donor-acceptor polymers for organic photovoltaics, Prog. Polym. Sci., 70 (2017) 34-51.
[5] Y.-Z. Chen, W.-H. Li, L. Li, L.-N. Wang, Progress in organic photocatalysts, Rare Met., 37 (2018) 1-12.
[6] S. Antohe, S. Iftimie, L. Hrostea, V.A. Antohe, M. Girtan, A critical review of photovoltaic cells based on organic monomeric and polymeric thin film heterojunctions, Thin Solid Films, 642 (2017) 219-231.
[7] S.M. Menke, R.J. Holmes, Exciton diffusion in organic photovoltaic cells, Energy Environ. Sci., 7 (2014) 499-512.
[8] S. He, Z. Lu, Excitonic processes at organic heterojunctions, Sci. China Phys. Mech. Astron., 61 (2018) 027301.
[9] D. Ti, K. Gao, Z.-P. Zhang, L.-T. Qu, Conjugated polymers as hole transporting materials for solar cells, Chin. J. Polym. Sci., 38 (2020) 449-458.
[10] M. Chevrier, H. Hawashin, S. Richeter, A. Mehdi, M. Surin, R. Lazzaroni, P. Dubois, B. Ratier, J. Bouclé, S. Clément, Well-designed poly(3-hexylthiophene) as hole transporting material: a new opportunity for solid-state dye-sensitized solar cells, Synth. Met., 226 (2017) 157-163.
[11] F. Yang, J. Li, C. Li, W. Li, Improving electron transport in a double-cable conjugated polymer via parallel perylenetriimide design, Macromolecules, 52 (2019) 3689-3696.
[12] K. Mahmood, S. Sarwar, M.T. Mehran, Current status of electron transport layers in perovskite solar cells: materials and properties, RSC Adv., 7 (2017) 17044-17062.
[13] W. Hou, Y. Xiao, G. Han, J.-Y. Lin, The applications of polymers in solar cells: a review, Polymers, 11 (2019) 143.
[14] L. Steier, S. Holliday, A bright outlook on organic photoelectrochemical cells for water splitting, J. Mater. Chem. A, 6 (2018) 21809-21826.
[15] T. Bourgeteau, D. Tondelier, B. Geffroy, R. Brisse, S. Campidelli, R. Cornut, B. Jousselme, All solution-processed organic photocathodes with increased efficiency and stability via the tuning of the hole-extracting layer, J. Mater. Chem. A, 4 (2016) 4831-4839.
[16] W. Shi, W. Yu, D. Li, D. Zhang, W. Fan, J. Shi, C. Li, PTB7:PC61BM Bulk heterojunction-based photocathodes for efficient hydrogen production in aqueous solution, Chem. Mater., 31 (2019) 1928-1935.
[17] S. Bellani, L. Najafi, A. Capasso, A.E. Del Rio Castillo, M.R. Antognazza, F. Bonaccorso, Few-layer MoS2 flakes as a hole-selective layer for solution-processed hybrid organic hydrogen-evolving photocathodes, J. Mater. Chem. A, 5 (2017) 4384-4396.
[18] M. Haro, C. Solis, G. Molina, L. Otero, J. Bisquert, S. Gimenez, A. Guerrero, Toward stable solar hydrogen generation using organic photoelectrochemical cells, J. Phys. Chem. C, 119 (2015) 6488-6494.
[19] E. Lanzarini, M.R. Antognazza, M. Biso, A. Ansaldo, L. Laudato, P. Bruno, P. Metrangolo, G. Resnati, D. Ricci, G. Lanzani, Polymer-based photocatalytic hydrogen generation, J. Phys. Chem. C, 116 (2012) 10944-10949.
[20] E. Nasybulin, M. Cox, I. Kymissis, K. Levon, Electrochemical codeposition of poly(thieno[3,2-b]thiophene) and fullerene: an approach to a bulk heterojunction organic photovoltaic device, Synth. Met., 162 (2012) 10-17.
[21] C. Solis, M.B. Ballatore, M.B. Suarez, M.E. Milanesio, E.N. Durantini, M. Santo, T. Dittrich, L. Otero, M. Gervaldo, Electrochemical generation of a molecular heterojunction. A new Zn-porphyrin-fullerene C60 polymeric film, Electrochim. Acta, 238 (2017) 81-90.
[22] M.B. Suarez, J. Durantini, L. Otero, T. Dittrich, M. Santo, M.E. Milanesio, E. Durantini, M. Gervaldo, Electrochemical generation of porphyrin-porphyrin and porphyrin-C60 polymeric photoactive organic heterojunctions, Electrochim. Acta, 133 (2014) 399-406.
[23] J. Durantini, M.B. Suarez, M. Santo, E. Durantini, T. Dittrich, L. Otero, M. Gervaldo, Photoinduced charge separation in organic–organic heterojunctions based on porphyrin electropolymers. Spectral and time dependent surface photovoltage study, J. Phys. Chem. C, 119 (2015) 4044-4051.
[24] D. Heredia, S.R. Martínez, A.M. Durantini, M.E. Pérez, M.I. Mangione, J.E. Durantini, M. Gervaldo, L.A. Otero, E.N. Durantini, Antimicrobial photodynamic polymeric films bearing biscarbazol-triphenylamine end-capped dendrimeric Zn(II) porphyrin, ACS Appl. Mater. Interfaces, 11 (2019) 27574-27587.
[25] D.A. Heredia, E.J. Gonzalez Lopez, E.N. Durantini, J. Durantini, T. Dittrich, J. Rappich, L. Macor, C. Solis, G.M. Morales, M. Gervaldo, L. Otero, Electrochemical, spectroelectrochemical and surface photovoltage study of ambipolar C60-EDOT and C60-carbazole based conducting polymers, Electrochim. Acta, 311 (2019) 178-191.

[26] Y. Zidon, Y. Shapira, T. Dittrich, Modulated charge separation at tetraphenyl porphyrin/Au interfaces, Appl. Phys. Lett., 90 (2007) 142103.
[27] M. Otero, T. Dittrich, J. Rappich, D.A. Heredia, F. Fungo, E. Durantini, L. Otero, Photoinduced charge separation in organic-inorganic hybrid system: C60-containing electropolymer / CdSe-quantum dots, Electrochim. Acta, 173 (2015) 316-322.
[28] V. Duzhko, V.Y. Timoshenko, F. Koch, T. Dittrich, Photovoltage in nanocrystalline porous TiO2, Phys. Rev. B, 64 (2001) 075204.
[29] S.-H. Hsiao, J.-C. Hsueh, Electrochemical synthesis and electrochromic properties of new conjugated polycarbazoles from di(carbazol-9-yl)-substituted triphenylamine and N-phenylcarbazole derivatives, J. Electroanal. Chem., 758 (2015) 100-110.
[30] J.F. Ambrose, R.F. Nelson, Anodic oxidation pathways of carbazoles: i. Carbazole and N- substituted derivatives, J. Electrochem. Soc., 115 (1968) 1159-1164.
[31] J. Durantini, L. Otero, M. Funes, E.N. Durantini, F. Fungo, M. Gervaldo. Electrochemical oxidation-induced polymerization of 5,10,15,20-tetrakis[3-(N-ethylcarbazoyl)]porphyrin. Formation and characterization of a novel electroactive porphyrin thin film, Electrochim. Acta 56 (2011) 4126-4134
[32] D. Dolphin, The Porphyrins, 1st Edition ed., Elsevier, Academic Press, 1978.
[33] H. Imahori, K. Tamaki, Y. Araki, Y. Sekiguchi, O. Ito, Y. Sakata, S. Fukuzumi, Stepwise Charge Separation and Charge Recombination in Ferrocene-meso,meso-Linked Porphyrin Dimer−Fullerene Triad, J. Am. Chem. Soc. 124 (2002) 5165-5174.
[34] M.I. Mangione, R.A. Spanevello, D. Minudri, D. Heredia, L. Fernandez, L. Otero, F. Fungo, Electropolimerization of functionalizaed carbazole end-capped dendrimers. formation of conductive films, Electrochim. Acta, 207 (2016) 143-151.
[35] W.-D. Quan, A. Pitto-Barry, L.A. Baker, E. Stulz, R. Napier, R.K. O'Reilly, V.G. Stavros, Retaining individualities: the photodynamics of self-ordering porphyrin assemblies, Chem. Commun., 52 (2016) 1938-1941.
[36] M. Gervaldo, P.A. Liddell, G. Kodis, B.J. Brennan, C.R. Johnson, J.W. Bridgewater, A.L. Moore, T.A. Moore, D. Gust, A photo- and electrochemically-active porphyrin–fullerene dyad electropolymer, Photochem. Photobiol. Sci., 9 (2010) 890-900.
[37] F. D'Souza, S. Gadde, D.M.S. Islam, C.A. Wijesinghe, A.L. Schumacher, M.E. Zandler, Y. Araki, O. Ito, Multi-triphenylamine-substituted porphyrin-fullerene conjugates as charge stabilizing "antenna−reaction center" mimics, J. Phys. Chem. A, 111 (2007) 8552-8560.
[38] Konev, A.F. Khlebnikov, P.I. Prolubnikov, A.S. Mereshchenko, A.V. Povolotskiy, O.V. Levin, A. Hirsch, Synthesis of new porphyrin–fullerene dyads capable of forming charge-separated states on a microsecond lifetime scale, Chem. Eur. J., 21 (2015) 1237-1250.
[39] N. von Morzé, T. Dittrich, W. Calvet, I. Lauermann, M. Rusu, Transient and modulated charge separation at CuInSe2/C60 and CuInSe2/ZnPc hybrid interfaces, Appl. Surf. Sci., 396 (2017) 366-374.
[40] F.E. Osterloh, M.A. Holmes, J. Zhao, L. Chang, S. Kawula, J.D. Roehling, A.J. Moulé, P3HT:PCBM Bulk-heterojunctions: observing interfacial and charge transfer states with surface photovoltage spectroscopy, J. Phys. Chem. C, 118 (2014) 14723-14731.
[41] M. Gervaldo, M. Funes, J. Durantini, L. Fernandez, F. Fungo, L. Otero, Electrochemical polymerization of palladium (II) and free base 5,10,15,20-tetrakis(4-N,Ndiphenylaminophenyl)porphyrins: Its applications as electrochromic and photoelectric materials, Electrochim. Acta 55 (2010) 1948-1957

Captions for Figures.

Fig. 1. Chemical structure of: a) m-Porp, b) m-C_{60}, and c) m-CBZ monomers. d) Schematic representation of the different electropolymerized layers that form the photoelectrode arrangements.

Fig. 2. Electrochemical growing of the layers that form the different photoelectrode arrangements: a) DCBZ/Porp/C_{60} d) DCBZ/Mix/C_{60}. Electrochemical responses of the layers that form the different photoelectrode arrangements: b) DCBZ/Porp/C_{60}, e) DCBZ/Mix/C_{60}. Absorption spectra of the layers that form the different photoelectrode arrangements: c) DCBZ/Porp/C_{60}, f) DCBZ/Mix/C_{60}. The layers were deposited over ITO.

Fig. 3. Difference absorption spectra, ΔAbs, of the layers that form the different photoelectrode arrangements on ITO electrodes obtained at applied potentials corresponding to the first and second oxidation peaks: a) and b) DCBZ/Porp/C_{60}; c) and d) DCBZ/Mix/C_{60}.

Fig. 4. Changes in the principal absorption traces of: a) DCBZ/Porp/C_{60} and b) DCBZ/Mix/C_{60} deposited on ITO electrodes, at the Soret band of porphyrin (420 nm), DCBZ radical cation (980 nm) and DCBZ di-cation (760 nm).

Fig. 5. Fluorescence emission spectra of: Porp (red line), Mix (black line), and Porp/C_{60} (blue line) layers deposited on ITO electrodes.

Fig. 6. SPV spectra of: a) DCBZ/Porp (red lines), DCBZ/Porp/C_{60} (blue lines), b) DCBZ/Mix (red lines), and c) DCBZ/Mix/C_{60} (blue lines) layers deposited on ITO electrodes, dashed lines in-phase and solid lines phase shifted by 90°.

Fig. 7. Photocurrent action spectra, IPCE% of: a) DCBZ, Porp, and C_{60}, b) DCBZ/Porp and DCBZ/Porp/C_{60}, and c) DCBZ/Mix and DCBZ/Mix/C_{60} layers deposited on ITO electrodes, in aqueous solution containing MV^{+2} (pH=7.5). Applied potential -200 mV.

Fig. 8. On-off illumination cycles of a) DCBZ/Porp/C_{60}, and b) DCBZ/Mix/C_{60} layers deposited on ITO electrodes, in aqueous solution (pH=4.5 without MV^{+2}). Applied potential -200 mV.

Fig. 9. Photocurrent action spectra, IPCE% of: a) DCBZ/Porp/C_{60}, and b) DCBZ/Mix/C_{60} layers deposited on ITO electrodes, in aqueous solution (pH=4.5 without MV^{+2}). Applied potential -200 mV.

Fig. 10. Energy levels diagram of the different layers in contact with MV^{+2} or H^{+}.

Fig.1.

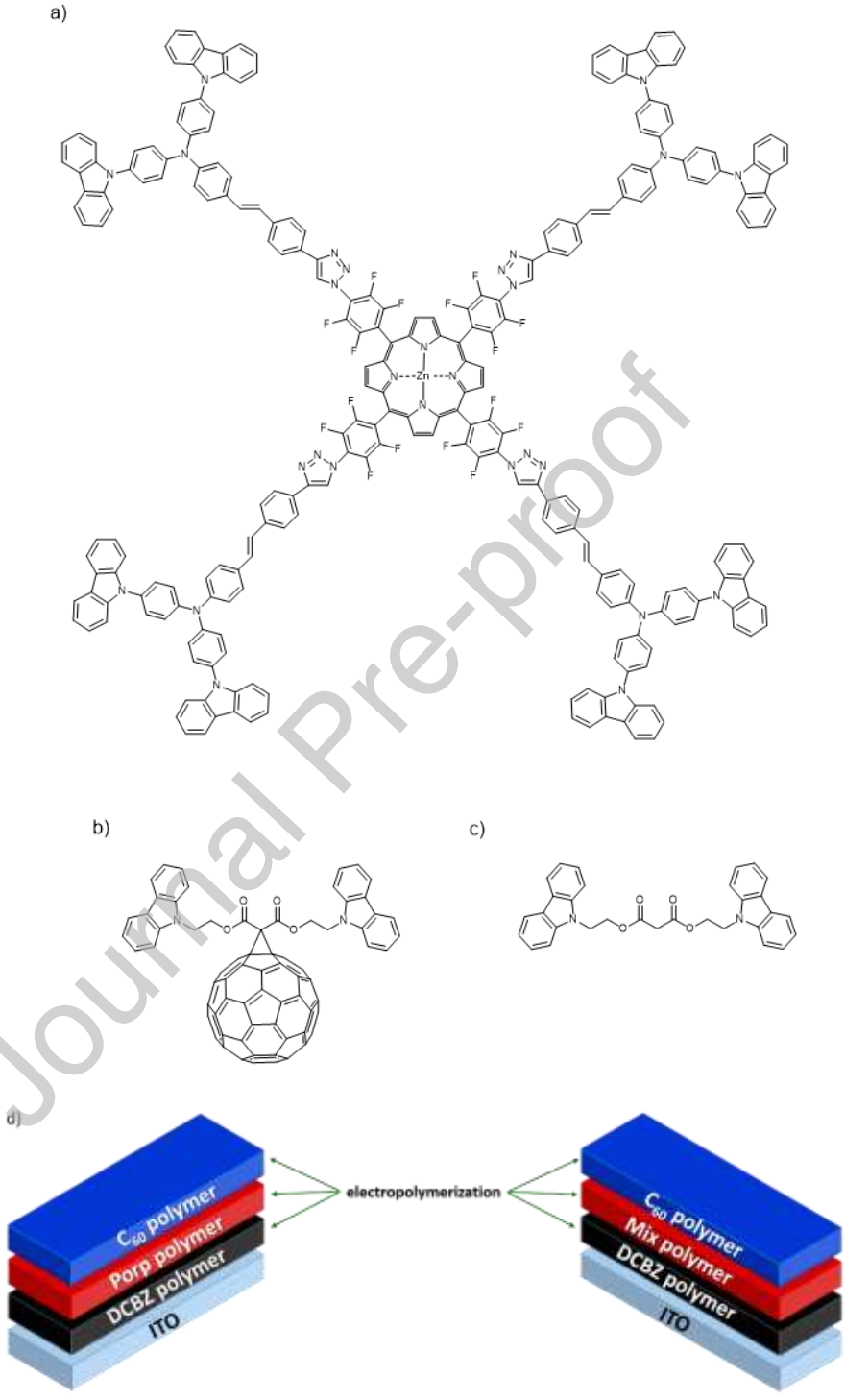

Fig. 2.

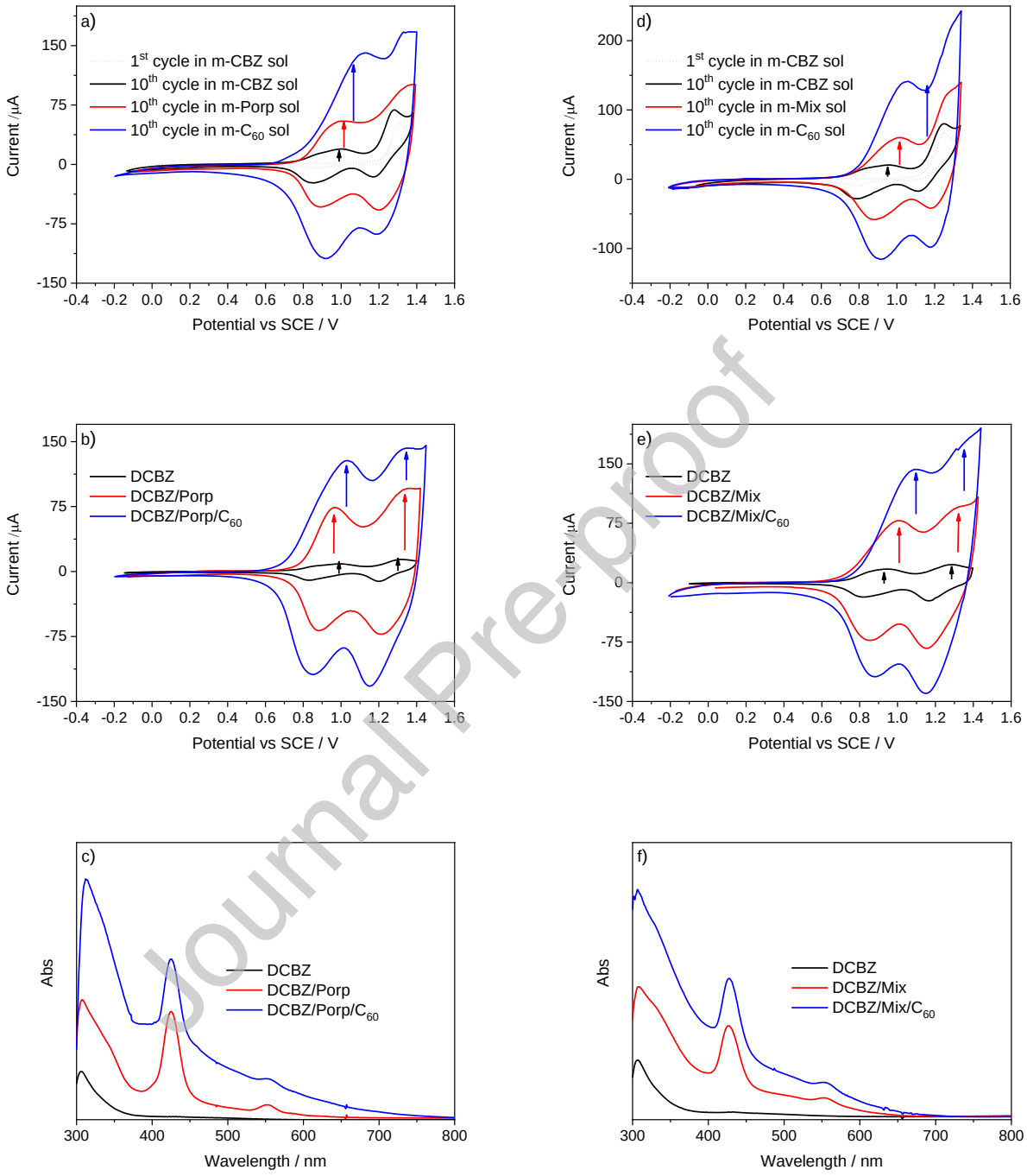

Fig. 3.

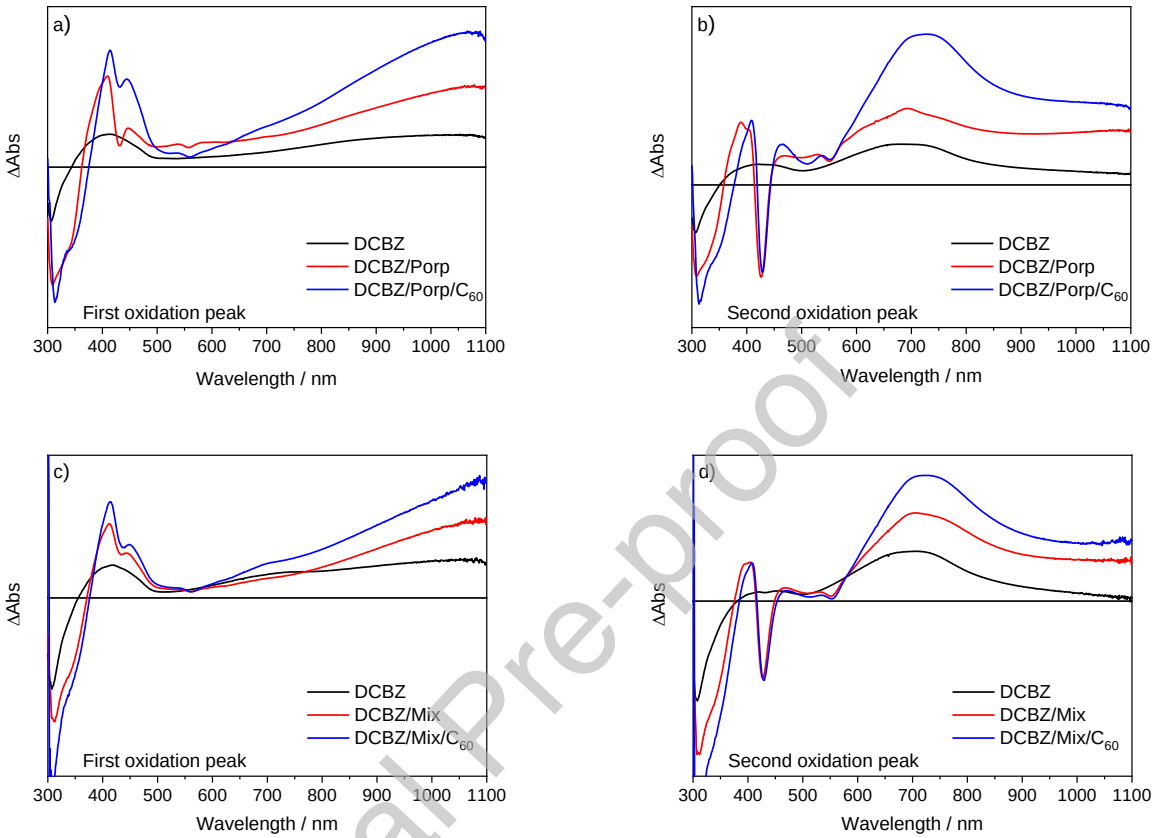

Fig. 4.

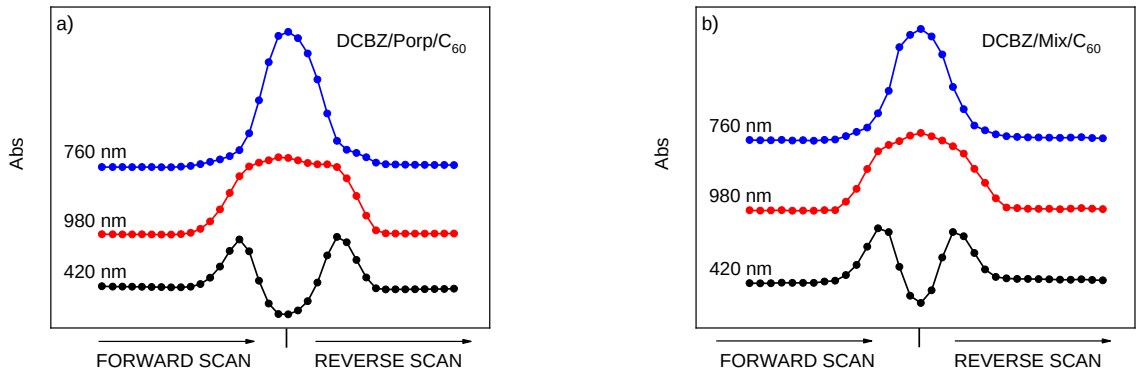

Fig. 5.

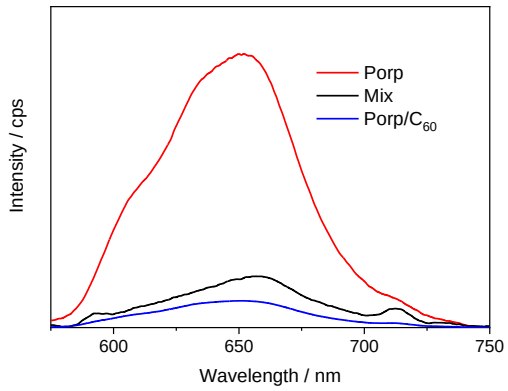

Fig. 6.

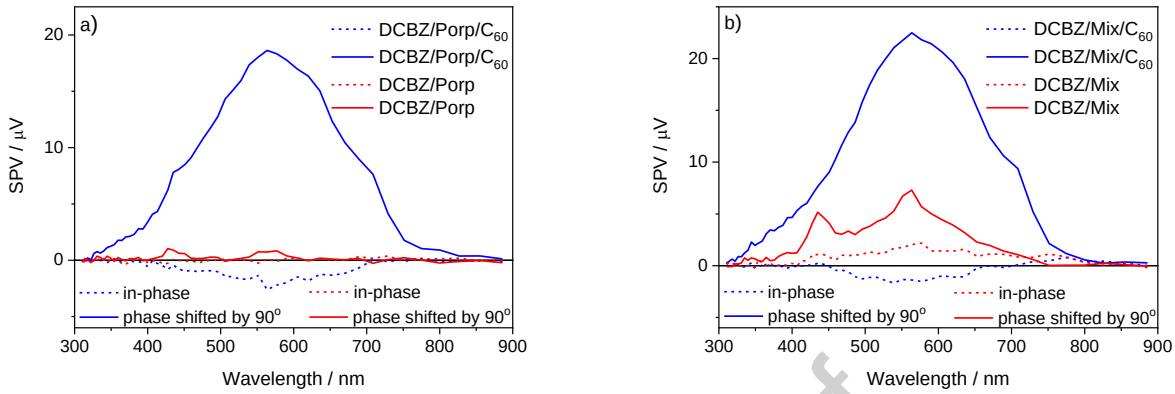

Fig. 7.

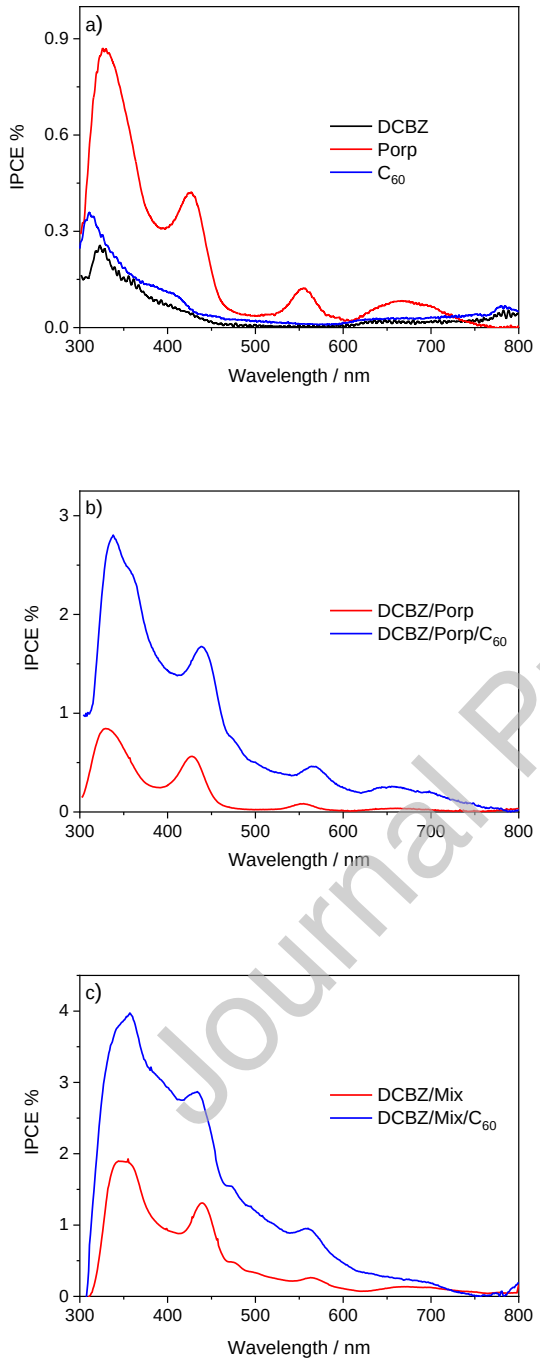

Fig. 8.

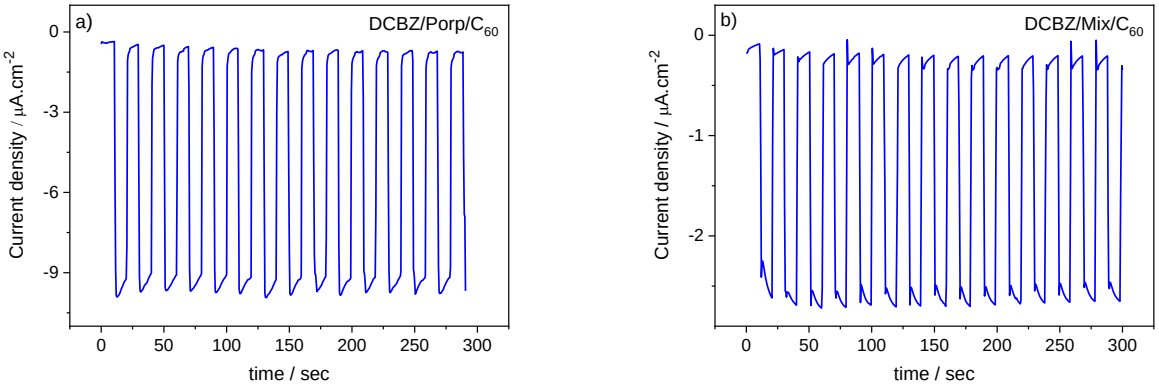

Fig. 9.

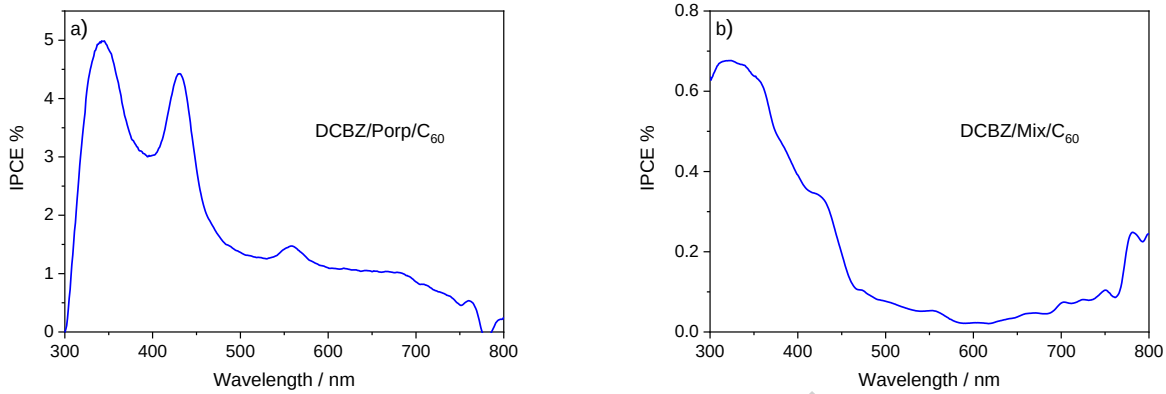

Fig. 10.

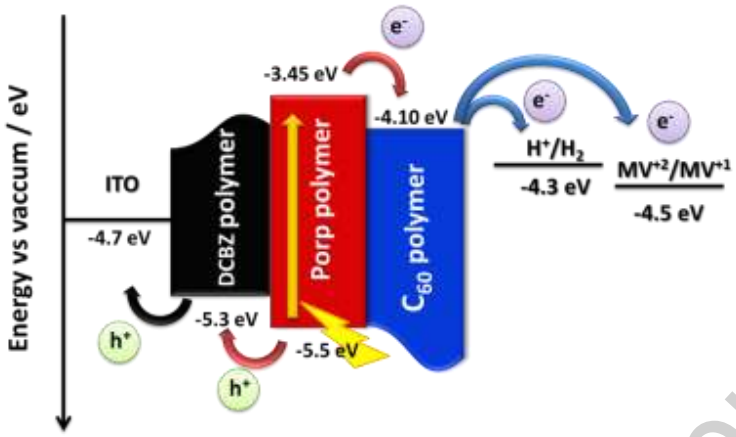

Graphical Abstract